AIAA SciTech Forum
January 3-7, 2022, San Diego, CA & Virtual
AIAA SCITECH 2022 Forum

10.2514/6.2022-0536

Aeroelastic Stability and Flow of Stresses in Wing Cross-Section

Mojtaba Moshtaghzadeh* and **Ehsan Izadpanahi†**
Florida International University, Miami, Florida 33174
Adrian Bejan‡
Duke University, Durham, North Carolina 27708-0300
Pezhman Mardanpour§
Florida International University, Miami, Florida 33174

The aeroelastic flight envelops of flying wing aircraft can be extended with a better flow of stresses in the structure. In the present study, we investigate the effect of cross-section configuration on the stress distribution and aeroelastic behavior of a flying wing aircraft. We invoke the constructal law and the principle; the prevention of stress strangulation leads to a wing design associated with the most stable and lightest structure. We used three computer programs Gmsh, VABS (Variational Asymptotic Beam Sectional Analysis), and NATASHA (Nonlinear Aeroelastic Trim And Stability of HALE Aircraft) to study stress distribution and stability of the flying wing aircraft. The results indicate that different wing cross-section designs affect stress distribution as well as the aeroelastic stability of the aircraft. Furthermore, the design with less stress strangulation is associated with a higher flutter speed structure.

Nomenclature

a	Deformed beam aerodynamic frame of reference
b	Undeformed beam cross-sectional frame of reference
B	Deformed beam cross-sectional frame of reference
$\mathbf{b}_i$	Unit vectors in undeformed beam cross-sectional frame of reference ($i = 1, 2, 3$)
$\mathbf{B}_i$	Unit vectors of deformed beam cross-sectional frame of reference ($i = 1, 2, 3$)
c	Chord
C^{bi}	Transformation matrix from the inertial frame i to deformed frame b
C^{Bi}	Transformation matrix from the inertial frame i to deformed frame B
C^{ib}	Transformation matrix from the undeformed frame b to inertial frame i
C^{iB}	Transformation matrix from the deformed frame B to inertial frame i
c_{d_0}, c_{l_0}	Aerodynamic drag and lift coefficients at zero angle of attack

*Graduate Research Assistant, Department of Mechanical and Material Engineering. Email: mmosh009@fiu.edu
†Postdoctoral Associate, Department of Mechanical and Material Engineering. Email: eizad001@fiu.edu
‡Professor, Department of Mechanical Engineering and Materials Science; abejan@duke.edu
§Assistant Professor, Department of Mechanical and Material Engineering. Member, AIAA. Email: Pezhman.Mardanpour@fiu.edu

$c_{m\beta}$	Pitch moment coefficient w.r.t. flap deflection (β)
$c_{l\alpha}$	Lift coefficient w.r.t. angle of attack (α)
$c_{l\beta}$	Lift coefficient w.r.t. flap deflection (β)
e_1	Column matrix
e	Offset of aerodynamic center from the origin of frame of reference along $\mathbf{b}_2$
f	Column matrix of distributed, applied force measured in $\mathbf{B}_i$ basis
F	Column matrix of internal force measured in $\mathbf{B}_i$ basis
$\mathbf{g}$	Gravitational vector in $\mathbf{B}_i$ basis
H	Column matrix of cross-sectional angular momentum measured in $\mathbf{B}_i$ basis
i	Inertial frame of reference
$\mathbf{i}_i$	Unit vectors for inertial frame of reference ($i = 1, 2, 3$)
I	Cross-sectional inertia matrix
k	Column matrix of undeformed beam initial curvature and twist measured in $\mathbf{b}_i$ basis
K	Column matrix of deformed beam curvature and twist measured in $\mathbf{B}_i$ basis
m	Column matrix of distributed, applied moment measured in $\mathbf{B}_i$ basis
M	Column matrix of internal moment measured in $\mathbf{B}_i$ basis
P	Column matrix of cross-sectional linear momentum measured in $\mathbf{B}_i$ basis
r	Column matrix of position vector measured in $\mathbf{b}_i$ basis
u	Column matrix of displacement vector measured in $\mathbf{b}_i$ basis
V	Column matrix of velocity measured in $\mathbf{B}_i$ basis
x_1	Axial coordinate of beam
α	Angle of attack
β	Trailing edge flap angle
γ	Column matrix of 1D generalized force strain measures
Δ	Identity matrix
κ	Column matrix of elastic twist and curvature measures (1D generalized moment strain measures)
λ	Column matrix of induced flow states
μ	Mass per unit length
ξ	Column matrix of center of mass offset from the frame of reference origin
ρ	Air density
ψ	Column matrix of small incremental rotations
$\mathbf{\Omega}$	Column matrix of cross-sectional angular velocity

$(\,)'$ Partial derivative with respect to x_1

$\dot{(\,)}$ Partial derivative with respect to time

$\hat{(\,)}$ Nodal variable

I. Introduction

Humans now require air vehicles that are more affordable and capable of flying faster and further. As a result, designers are constantly focusing on providing more energy-efficient vehicles. This phenomenon is characterized in thermodynamics in terms of the system's "energy-conversion efficiency": the higher the efficiency, the better the design [1]. The thermodynamics laws describe the phenomena of irreversibility and energy conservation. The *constructal law* explains the phenomenon of natural evolution and change: "For a finite-size flow system to persist in time (to live), its configuration must evolve in such a way that provides greater and greater access to the currents that flow through it" [2]. The constructal law provides a solution for a problem by predicting configurations without making any assumptions. Bejan et al. [3] demonstrated that design evolution is a natural and predictable phenomenon in nature.

Several successive constructal law applications in the evolutionary design of engineering and biological systems are presented in the books "Shape and Structure, from Engineering to Nature" and "Design with constructal theory" [4, 5]. Constructal law predicts the evolution of human-and-machine species such as helicopters, aircraft, and ships in which are perfect agreement with the evolution of animals [6–9]. We can study the evolution of airplanes (e.g., fuel load, speed, wings, fuselage, and engine) by employing theories derived from the Constructal law [10–12]. For example, "Large or small, airplanes exhibit a proportionality between wingspan and fuselage length, and between fuel load and body size" [1, 10]. The efficiency and stability of an aircraft can be significantly influenced by selecting the proper engine size; "this scaling is analogous to animal design, where the mass of the motive organs (muscles, heart, lungs) is proportional to the body size" [7].

In the design of airplane parts, a variety of strategies have been used [13–16]. Schumacher et al. [15] applied the Multidisciplinary Design Optimization (MDO) method in the design process of a wing box of a Fairchild Dornier regional jet family. Rao et al. [16] used a topology optimization method to find the best design of wing of Dornier aircraft, which was designed by considering the optimum material distribution and configuration. Hong Zhu et al. [17] studied topology optimization in a variety of aircraft aspects, including shape-preserving design in aerospace, dynamic responses, and aircraft body structure. These methods work by searching through predetermined configurations and selecting the best one that meets the design goals. According to the constructal law, the designer has no presumptions when discovering and constructing the configuration and derives the appropriate geometry from the principles. The constructal approach facilitates the design to improve [18].

The flow plays an essential part in evaluating a system. In flow systems, three main properties stand out: *what* flows through the system (fluid, heat, mass, stress, etc.), *how much* flows can transfer (flow rate, current, traffic, etc.), and *where* the stream is located (location and configuration). The *where* (geometry, configuration, and design) is the focus of the discoveries based on the constructal law [1, 19]. The main idea investigated by the constructal law is the location where the stream runs [20]. The stability of a flexible structure is affected by the strangulation (or concentration) of the flow of stresses. When the cross-section is homogeneous, the stress flows smoothly, resulting in the lightest and strongest structure possible[20]. To seek various wing cross-section configurations, we use the constructal law and the evolution of the flow of stresses in this work.

Mardanpour et al. [1] demonstrated how a design parameter like engine placement has a significant impact on aeroelastic stability and stress distribution in the aircraft's wings. Izadpanahi et al. [21, 22] found that if the flow of stresses is not strangled through wings of aircraft, higher flutter can be achieved. In addition, Moshtaghzadeh et al. [18, 22] investigated the relationship between aeroelastic instabilities and stress strangulation through the wing cross-section and the wing. It is demonstrated that circular and oval voids are the most effective designs, allowing stresses to flow easily around curved geometries.

In this paper, we derive an aeroelastic constructal theory to scale up (add complexity) to the design of the wing cross-section. We use the numerical simulation program Nonlinear Aeroelastic Trim And Stability of HALE Aircraft (NATASHA)[23, 24] to analyze the stability of the aircraft. This computer program benefits from the nonlinear composite beam theory of Hodges [25] and the finite induced flow model of Peters et al. [26]. NATASHA has been verified and validated with both experimental and numerical benchmarks [27–35]. The flow of stresses of the trimmed aircraft with different wing designs is recovered using Variational Asymptotic Beam Sectional Analysis (VABS). Finally, the contour of each stress tensor component will be plotted, and the relationship with the flutter characteristics will be explored.

II. Theory

A. Nonlinear Composite Beam Theory

The fully intrinsic nonlinear composite beam theory is based on first-order partial differential equations of motion for the beam, which are independent of displacement and rotation variables. The equations contain variables that are expressed in terms of the bases of the reference frames for the undeformed and deformed beams, $b(x_1)$ and $B(x_1, t)$, respectively; see Fig. 1. These equations are based on force, moment, angular velocity, and velocity with nonlinearities

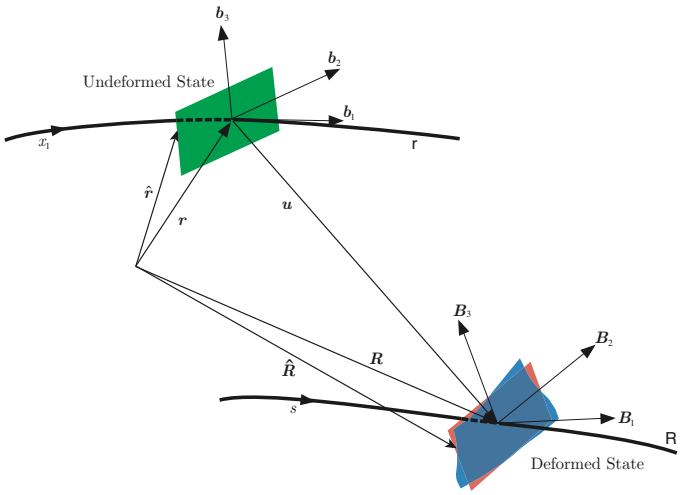

Fig. 1 The essential features of beam kinematics [25].

of second order. The equations of motion are:

$$\begin{aligned} F_B' + \widetilde{K}_B F_B + f_B &= \dot{P}_B + \widetilde{\Omega}_B P_B \\ M_B' + \widetilde{K}_B M_B + (\widetilde{e}_1 + \widetilde{\gamma}) F_B + m_B &= \dot{H}_B + \widetilde{\Omega}_B H_B + \widetilde{V}_B P_B \end{aligned} \tag{1}$$

where the generalized strains and velocities are related to stress resultants and moments by the structural constitutive equations

$$\begin{Bmatrix} \gamma \\ \kappa \end{Bmatrix} = \begin{bmatrix} R & S \\ S^T & T \end{bmatrix} \begin{Bmatrix} F_B \\ M_B \end{Bmatrix} \tag{2}$$

and the inertial constitutive equations

$$\begin{Bmatrix} P_B \\ H_B \end{Bmatrix} = \begin{bmatrix} \mu\Delta & -\mu\widetilde{\xi} \\ \mu\widetilde{\xi} & I \end{bmatrix} \begin{Bmatrix} V_B \\ \Omega_B \end{Bmatrix}. \tag{3}$$

Finally, strain- and velocity-displacement equations are used to derive the intrinsic kinematical partial differential equations [25], which are given as

$$\begin{aligned} V_B' + \widetilde{K}_B V_B + (\widetilde{e}_1 + \widetilde{\gamma}) \Omega_B &= \dot{\gamma} \\ \Omega_B' + \widetilde{K}_B \Omega_B &= \dot{\kappa} \end{aligned} \tag{4}$$

In this set of equations, F_B and M_B are column matrices of cross-sectional stress and moment resultant measures in the B frame, respectively; V_B and Ω_B are column matrices of cross-sectional frame velocity and angular velocity measures in the B frame, respectively; P_B and H_B are column matrices of cross-sectional linear and angular momentum measures in the B frame, respectively; R, S, and T are 3×3 partitions of the cross-sectional flexibility matrix; Δ is the 3×3 identity matrix; I is the 3×3 cross-sectional inertia matrix; ξ is $\lfloor 0 \;\; \xi_2 \;\; \xi_3 \rfloor^T$ with ξ_2 and ξ_3 representing the position coordinates

of the cross-sectional mass center with respect to the reference line; μ is the mass per unit length; $\widetilde{(\,)}$ denotes the antisymmetric 3×3 matrix associated with the column matrix over which the tilde is placed; $\dot{(\,)}$ denotes the partial derivative with respect to time; and $(\,)'$ denotes the partial derivative with respect to the axial coordinate, x_1. More details about these equations can be found in Ref. [36]. This is a complete set of first-order, partial differential equations. To solve the system of equations, one may eliminate γ and κ using Eq. (3) and P_B and H_B using Eq. (4). Then, 12 boundary conditions are needed in terms of force (F_B), moment (M_B), velocity (V_B) and angular velocity (Ω_B). The maximum degree of nonlinearities is two, and because displacement and rotation variables do not appear, singularities caused by finite rotations are avoided. If needed, the position and the orientation can be calculated as post-processing operations by integrating

$$\begin{aligned} r_i' &= C^{ib} e_1 \\ r_i + u_i' &= C^{iB}(e_1 + \gamma) \end{aligned} \tag{5}$$

and

$$\begin{aligned} (C^{bi})' &= -\widetilde{k} C^{bi} \\ (C^{Bi})' &= -(\widetilde{k} + \widetilde{\kappa}) C^{Bi} \end{aligned} \tag{6}$$

Here C defines the transformation matrix, r is column matrix of position vector measured in $\mathbf{b}_i$ basis, and u indicates the column matrix of displacement vector measured in $\mathbf{b}_i$ basis [18].

B. Finite State Induced Model

The two-dimensional finite state aerodynamic model of Peters et al. [26]is a state-space, thin-airfoil, inviscid, incompressible approximation of an infinite-state representation of the aerodynamic loads, which accounts for induced flow in the wake and apparent mass effects, using known airfoil parameters. It accommodates large motion of the airfoil as well as deflection of a small trailing-edge flap. Although the two-dimensional version of this model does not account for three-dimensional effects associated with the wing tip, published data [26, 27, 30] show that this theory is an excellent approximation of aerodynamic loads acting on high-aspect ratio wings. The lift, drag and pitching moment at the quarter-chord are given by:

$$L_{aero} = \rho b \left[\left(c_{l_0} + c_{l_\beta} \beta \right) V_T V_{a_2} - c_{l_\alpha} \dot{V}_{a_3} \, b/2 - c_{l_\alpha} V_{a_2} \left(V_{a_3} + \lambda_0 - \Omega_{a_1} b/2 \right) - c_{d_o} V_T V_{a_3} \right] \tag{7}$$

$$D_{aero} = \rho b \left[- \left(c_{l_0} + c_{l_\beta} \beta \right) V_T V_{a_3} + c_{l_\alpha} \left(V_{a_3} + \lambda_0 \right)^2 - c_{d_o} V_T V_{a_2} \right] \tag{8}$$

$$M_{aero} = 2\rho b \left[\left(c_{m_0} + c_{m_\beta} \beta \right) V_T - c_{m_\alpha} V_T V_{a_3} - b c_{l_\alpha} / 8 V_{a_2} \Omega_{a_1} - b^2 c_{l_\alpha} \dot{\Omega}_{a_1} / 32 + b c_{l_\alpha} \dot{V}_{a_3} / 8 \right] \tag{9}$$

$$V_T = (V_{a_2}^2 + V_{a_3}^2)^{1/2}. \tag{10}$$

$$\sin\alpha = \frac{-V_{a_3}}{V_T} \tag{11}$$

$$\alpha_{rot} = \frac{\Omega_{a_1} b/2}{V_T} \tag{12}$$

and V_{a_2}, V_{a_3} are the measured values of V_a, and β is the angle of flap deflection. The effect of unsteady wake (induced flow) and apparent mass appear as λ_0 and acceleration terms in the force and moment equations. The induced flow model of Peters et al. [26] is included to calculate λ_0 as,

$$[A_{\text{induced flow}}]\{\dot{\lambda}\} + \left(\frac{V_T}{b}\right)\{\lambda\} = \left(-\dot{V}_{a_3} + \frac{b}{2}\dot{\Omega}_{a_1}\right)\{c_{\text{induced flow}}\} \tag{13}$$

$$\lambda_0 = \frac{1}{2}\left\{b_{induced\ flow}\right\}^T \{\lambda\} \tag{14}$$

where λ is the column matrix of induced flow states, and $\left[A_{induced\ flow}\right]$, $\left\{c_{induced\ flow}\right\}$, $\left\{b_{induced\ flow}\right\}$ are constant matrices derived in Ref.[26] [18].

C. Aeroelastic System

The aeroelastic system is described by coupling the aerodynamic equations with the structural equations,

$$[A]\{\dot{x}\} + \{B(x)\} = \{f_{cont}\} \tag{15}$$

where, $\{x\}$ and f_{cont} represent the vector of all the aeroelastic variables and the vector of the flight controls, respectively. The resulting nonlinear ordinary differential equations are linearized about a static equilibrium state. The equilibrium state is governed by nonlinear algebraic equations, which the code NATASHA solves in obtaining the steady-state trim solution using the Newton-Raphson procedure [23]. This system of nonlinear aeroelastic equations, when linearized about the resulting trim state, leads to a standard eigenvalue problem, which NATASHA uses to analyze the stability of the structure. The linearized system can be represented as

$$[A]\left\{\dot{\hat{x}}\right\} + [B]\left\{\hat{x}\right\} = \left\{\hat{f}_{cont}\right\} \tag{16}$$

where $\hat{(\ )}$ indicates the perturbation about the steady-state values [18].

D. Variational Asymptotic Beam Sectional Analysis (VABS)

VABS [37-39] is a commercial software that uses the variational method to simplify a 3D nonlinear analysis. It projects 3D slender structures to a two-dimensional (2D) cross-sectional and one dimensional (1D) beam analysis. VABS decreases the analysis time from hours to seconds while maintaining the accuracy of detailed 3D FEA. It uses a finite element mesh of the cross-section and material properties as inputs to calculate the cross-sectional properties (e.g., structural properties and inertial properties). It also performs stress recovery using inputs such as axial and shear forces, moments, distributed forces, and moments including applied and inertial [18].

III. Numerical Simulation

We employed three computer programs, Gmsh [40], VABS, NATASHA, and several functions and scripts are developed in MATLAB to connect these software packages and perform the postprocessing of stresses [18]. In this study, we used Gmsh software to mesh the cross-section of a flying aircraft. Then, we used VABS to find the cross-sectional properties of the fuselage and wings of the aircraft. We utilized these properties as inputs in the computer program NATASHA to evaluate the stability analysis and find the trim state results. Finally, the results are fed into the VABS software, which calculates the stresses in the wings. Figure 2 shows the numerical simulation procedure in this paper.

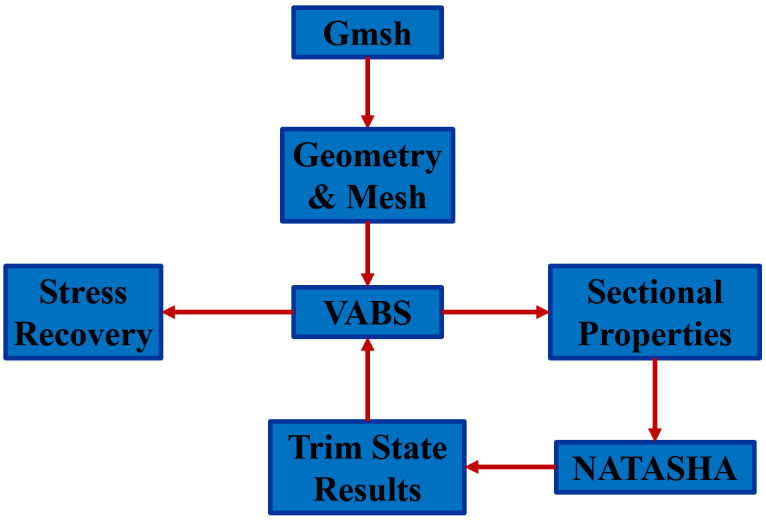

Fig. 2 The simulation procedure.

In this study, the aircraft has two wings and a fuselage measuring 18 m and 4 m in length. We studied the airfoil NACA0012 with a 1 m chord. The fuselage has four elements, and each wing has 18 elements. From the center to the root of each wing, the fuselage is linearly tapered and considered as a rigid body. The aircraft includes two engines, each with a mass of 10 kg, mounted on the fuselage. For each wing, nine flaps are considered, distributed between the mid-span and the tip of the wings. The wings are swept with 15^o backward. Fig. 3 depicts a schematic view of the designed aircraft and Table 1 includes a list of aerodynamic properties.

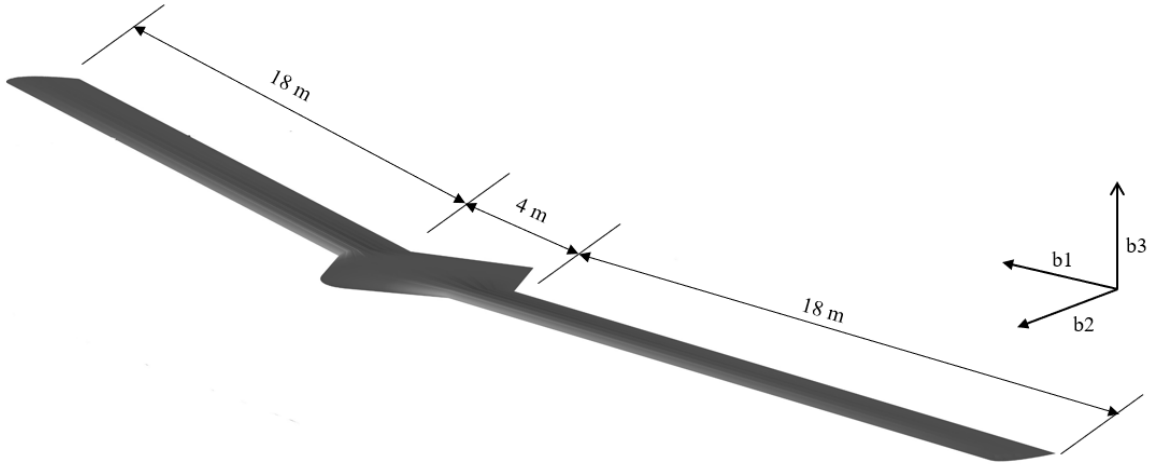

Fig. 3 3D view of the flying wing aircraft.

Property	e [m]	c_{l_α}	c_{l_β}	c_{d_0}	c_{m_0}	c_{m_α}	c_{m_β}	$\rho\ [kg.m^{-3}]$
Value	0.25	2π	1	0.01	0.0	-0.08	-0.25	0.0889

Table 1 The aerodynamic properties and coefficients of the wings.

Tables 2- 3 provide the mechanical properties of the proposed configurations in this study. Table 4 shows these six cross-sectional configurations. Case I contains a thick strip in the $\mathbf{b}_2$ direction. The thickness of this strip decreases in case II. The removed mass is added to the branches in the plunge direction ($\mathbf{b}_3$). In addition, the configuration of cases V and VI is inspired by bird's wing [41].

IV. Results and Discussion

First, we examine the flying wing aircraft's stability in each of the six cases. Then, we investigate the flow of stresses through the wing while keeping the overall mass in each cross-section the same.

In the configurations I to II, we study the flow of stresses as the stress pathways are morphed from the lead-lag ($\mathbf{b}_2$) to the plunge direction ($\mathbf{b}_3$). Decreasing the pathway in the lead-lag direction and increasing the thickness in the plunge direction could improve the aeroelastic stability of the aircraft. We focus on enhancing the flow of stresses in the $\mathbf{b}_3$ direction in configurations II to VI by morphing the stress paths toward smoother geometries. We discovered that σ_{11}, σ_{12}, σ_{13} are the most dominant stresses. These results are consistent with our earlier studies [18, 22, 42–44]. Therefore, σ_{11}, σ_{12}, σ_{13}, and Von Mises stresses are presented in this paper.

The flutter speed and frequency are presented in Table 4. These findings show that changing the wing cross-section configuration considerably improves the stability of a flying wing aircraft. Comparing cases I and II demonstrates that

Property	Case I	Case II	Case III
Span $[m]$	20	20	20
R $[N^{-1}]$	$\begin{bmatrix} 3.80\times10^{-9} & 0 & 0 \\ 0 & 1.20\times10^{-8} & 3.54\times10^{-12} \\ 0 & 3.54\times10^{-12} & 1.20\times10^{-7} \end{bmatrix}$	$\begin{bmatrix} 3.90\times10^{-9} & 0 & 0 \\ 0 & 1.65\times10^{-8} & -3.99\times10^{-13} \\ 0 & -3.99\times10^{-13} & 9.16\times10^{-8} \end{bmatrix}$	$\begin{bmatrix} 3.91\times10^{-9} & 0 & 0 \\ 0 & 1.65\times10^{-8} & 2.42\times10^{-12} \\ 0 & 2.42\times10^{-12} & 1.04\times10^{-7} \end{bmatrix}$
S $[N^{-1}.m^{-1}]$	$\begin{bmatrix} 0 & 3.60\times10^{-14} & 2.56\times10^{-9} \\ 2.55\times10^{-13} & 0 & 0 \\ -4.13\times10^{-7} & 0 & 0 \end{bmatrix}$	$\begin{bmatrix} 0 & -3.37\times10^{-14} & 3.30\times10^{-9} \\ 1.27\times10^{-11} & 0 & 0 \\ -4.11\times10^{-7} & 0 & 0 \end{bmatrix}$	$\begin{bmatrix} 0 & 5.06\times10^{-14} & 3.32\times10^{-9} \\ -1.28\times10^{-11} & 0 & 0 \\ -4.50\times10^{-7} & 0 & 0 \end{bmatrix}$
T $[N^{-1}.m^{-2}]$	$\begin{bmatrix} 3.552\times10^{-6} & 0 & 0 \\ 0 & 4.892\times10^{-6} & 6.521\times10^{-13} \\ 0 & 6.521\times10^{-13} & 5.464\times10^{-8} \end{bmatrix}$	$\begin{bmatrix} 3.24\times10^{-6} & 0 & 0 \\ 0 & 4.08\times10^{-6} & -1.42\times10^{-13} \\ 0 & -1.42\times10^{-13} & 5.69\times10^{-8} \end{bmatrix}$	$\begin{bmatrix} 3.26\times10^{-6} & 0 & 0 \\ 0 & 4.09\times10^{-6} & 4.17\times10^{-13} \\ 0 & 4.17\times10^{-13} & 5.66\times10^{-8} \end{bmatrix}$
I $[kg.m]$	$\begin{bmatrix} 3.86\times10^{-1} & 0 & 0 \\ 0 & 4.10\times10^{-3} & 1.83\times10^{-11} \\ 0 & 1.83\times10^{-11} & 3.82\times10^{-1} \end{bmatrix}$	$\begin{bmatrix} 3.57\times10^{-1} & 0 & 0 \\ 0 & 4.93\times10^{-3} & 1.63\times10^{-13} \\ 0 & 1.63\times10^{-13} & 3.52\times10^{-1} \end{bmatrix}$	$\begin{bmatrix} 3.58\times10^{-1} & 0 & 0 \\ 0 & 4.93\times10^{-3} & -5.12\times10^{-13} \\ 0 & -5.12\times10^{-13} & 3.53\times10^{-1} \end{bmatrix}$
ξ $[m]$	$\begin{bmatrix} 0 \\ 5.26\times10^{-2} \\ -3.23\times10^{-19} \end{bmatrix}$	$\begin{bmatrix} 0 \\ 6.36\times10^{-2} \\ -6.51\times10^{-20} \end{bmatrix}$	$\begin{bmatrix} 0 \\ 6.41\times10^{-2} \\ -1.30\times10^{-19} \end{bmatrix}$
Mass $[kg.m^{-1}]$	5.514	5.514	5.512
Chord $[m]$	1	1	1

Table 2 The cross sectional properties of the wings for cases I, II and III in SI unit system.

Property	Case IV	Case V	Case VI
Span $[m]$	20	20	20
R $[N^{-1}]$	$\begin{bmatrix} 4.33\times10^{-9} & 0 & 0 \\ 0 & 1.31\times10^{-8} & 1.79\times10^{-9} \\ 0 & 1.79\times10^{-8} & 2.55\times10^{-7} \end{bmatrix}$	$\begin{bmatrix} 4.17\times10^{-9} & 0 & 0 \\ 0 & 1.57\times10^{-8} & -5.18\times10^{-9} \\ 0 & -5.18\times10^{-9} & 1.11\times10^{-7} \end{bmatrix}$	$\begin{bmatrix} 4.33\times10^{-9} & 0 & 0 \\ 0 & 1.30\times10^{-8} & 1.79\times10^{-9} \\ 0 & 1.79\times10^{-9} & 2.55\times10^{-7} \end{bmatrix}$
S $[N^{-1}.m^{-1}]$	$\begin{bmatrix} 0 & -1.10\times10^{-8} & 6.09\times10^{-9} \\ 1.41\times10^{-8} & 0 & 0 \\ -6.01\times10^{-7} & 0 & 0 \end{bmatrix}$	$\begin{bmatrix} 0 & -4.77\times10^{-9} & 5.09\times10^{-9} \\ 3.01\times10^{-8} & 0 & 0 \\ -4.76\times10^{-7} & 0 & 0 \end{bmatrix}$	$\begin{bmatrix} 0 & -1.10\times10^{-8} & 6.09\times10^{-9} \\ 1.41\times10^{-8} & 0 & 0 \\ -6.01\times10^{-7} & 0 & 0 \end{bmatrix}$
T $[N^{-1}.m^{-2}]$	$\begin{bmatrix} 3.09\times10^{-6} & 0 & 0 \\ 0 & 3.98\times10^{-6} & -2.29\times10^{-8} \\ 0 & -2.29\times10^{-8} & 6.03\times10^{-8} \end{bmatrix}$	$\begin{bmatrix} 3.22\times10^{-6} & 0 & 0 \\ 0 & 4.05\times10^{-6} & -9.68\times10^{-9} \\ 0 & -9.68\times10^{-9} & 6.05\times10^{-8} \end{bmatrix}$	$\begin{bmatrix} 3.09\times10^{-6} & 0 & 0 \\ 0 & 3.98\times10^{-6} & -2.29\times10^{-8} \\ 0 & -2.29\times10^{-8} & 6.03\times10^{-8} \end{bmatrix}$
I $[kg.m]$	$\begin{bmatrix} 3.36\times10^{-1} & 0 & 0 \\ 0 & 5.07\times10^{-3} & 1.96\times10^{-3} \\ 0 & 1.96\times10^{-3} & 3.31\times10^{-1} \end{bmatrix}$	$\begin{bmatrix} 3.34\times10^{-1} & 0 & 0 \\ 0 & 4.98\times10^{-3} & 8.21\times10^{-4} \\ 0 & 8.21\times10^{-4} & 3.29\times10^{-1} \end{bmatrix}$	$\begin{bmatrix} 3.36\times10^{-1} & 0 & 0 \\ 0 & 5.07\times10^{-3} & 1.96\times10^{-3} \\ 0 & 1.96\times10^{-3} & 3.31\times10^{-1} \end{bmatrix}$
ξ $[m]$	$\begin{bmatrix} 0 \\ 6.56\times10^{-2} \\ 8.36\times10^{-20} \end{bmatrix}$	$\begin{bmatrix} 0 \\ 8.91\times10^{-2} \\ 9.47\times10^{-4} \end{bmatrix}$	$\begin{bmatrix} 0 \\ 1.05\times10^{-1} \\ 2.20\times10^{-3} \end{bmatrix}$
Mass $[kg.m^{-1}]$	5.513	5.531	5.587
Chord $[m]$	1	1	1

Table 3 Properties of the wings for cases IV, V and VI in SI units system.

changing the mass concentration from the $\mathbf{b}_2$ direction to the $\mathbf{b}_3$ direction increases the flutter speed. Although using curve branches in $\mathbf{b}_3$ could increase the flutter speed in cases II to IV, this improvement is not significant. Finally, it is shown that moving the mass center to the leading edge could enhance the flutter speed significantly from case V to VI.

Case	Cross-Section	Flutter Speed [m/s]	Flutter Frequency [Hz]
I		43.28	0.732
II		47.34	0.816
III		47.34	0.816
IV		47.50	0.816
V		48.59	0.834
VI		49.84	0.847

Table 4 Description of Cases.

In the following, we present how the stresses flow through the configurations and discuss the analogy between instability and stress distributions. We found the flow of stresses for all cases at a cruise speed of 40 m/s under the same flight state. Figures 4-7 present the flow of stresses of the wing cross-section configurations.

It is found from Fig. 4 that all the configurations are under compression at the upper surface and under tension at the lower surface of the wing. The magnitude of σ_{11} decreases and the distribution of this stress component becomes smoother from the case I to VI. σ_{12} and σ_{13} distributions are shown in Figs. 5-6. σ_{13} flows mainly in the stress-carrying pathways, in the $\mathbf{b}_2$ direction. By decreasing the thickness in the $\mathbf{b}_2$ direction, stress strangulation occurs. However, the magnitude of these stresses has substantially smaller values than σ_{11}: σ_{12} is one order of magnitude smaller, and σ_{13} is two orders of magnitude smaller than σ_{11}. These results demonstrate that σ_{11} has a significant impact on the aircraft's stability.

Figure 7 presents the Von Mises stress distribution. Case I has considerable stress strangulation at the root of the wing. This stress strangulation becomes smoother as we morph the configuration from case I to VI. Case VI reaches the highest flutter speed, associated with a smoother flow of stresses. It is found that the path in the $\mathbf{b}_2$ direction does not carry a significant amount of the flow of Von Mises stresses.

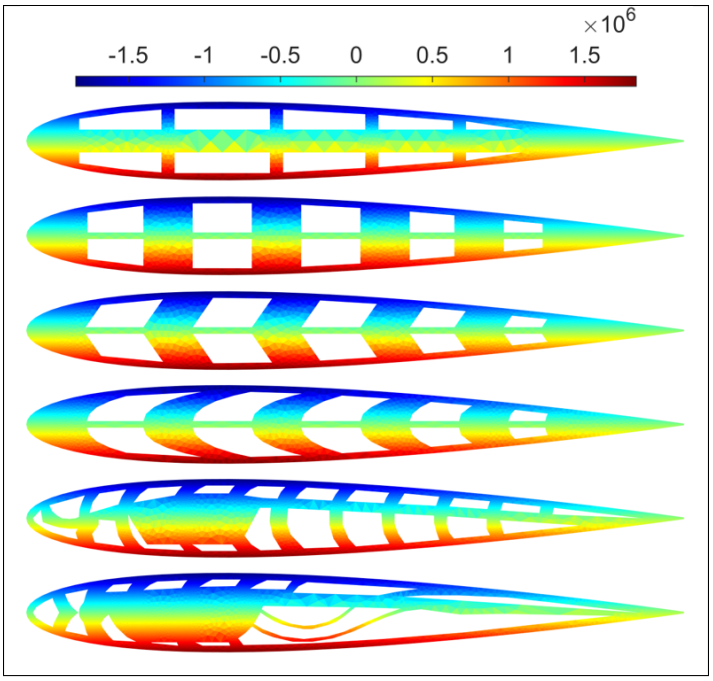

Fig. 4 σ_{11} **(pa) distribution of wing cross-section at the cruise speed of 40 m/s.**

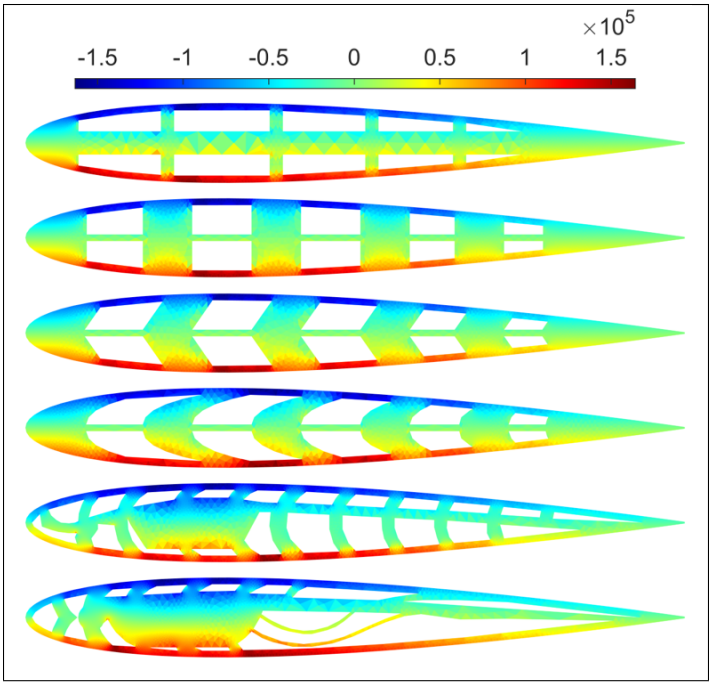

Fig. 5 σ_{12} **(pa) distribution of wing cross-section at the cruise speed of 40 m/s.**

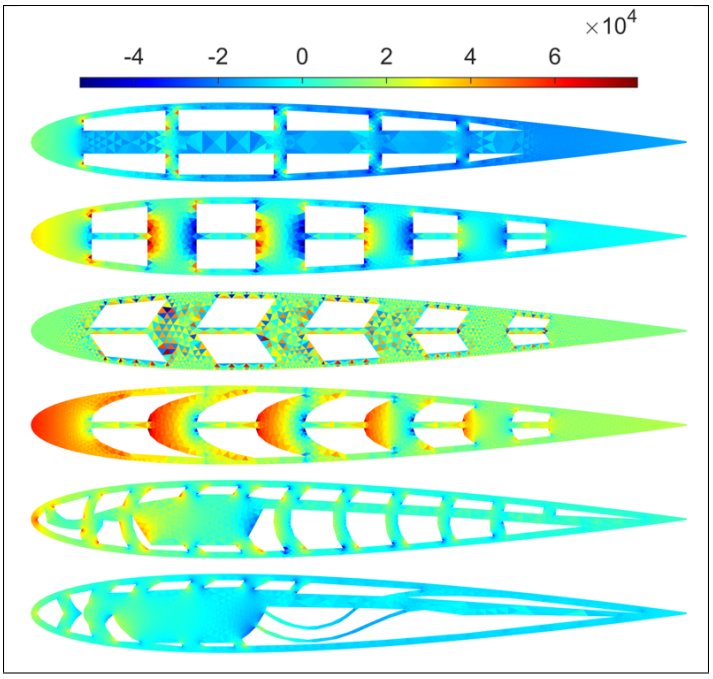

Fig. 6 σ_{13} **(pa) distribution of wing cross-section at the cruise speed of 40 m/s.**

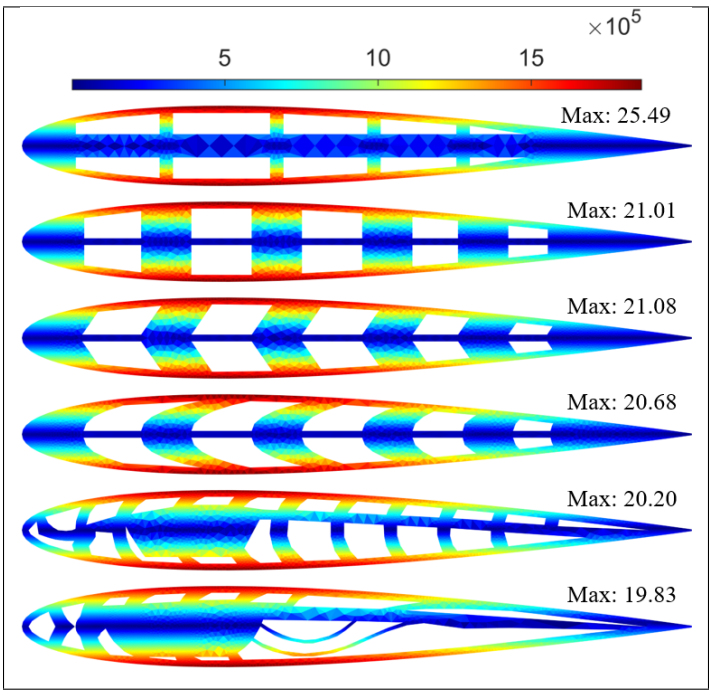

Fig. 7 Von Mises stress (pa) distribution of wing cross-section at the cruise speed of 40 m/s.

V. Conclusion

To examine the aeroelastic stability of six configurations of the cross-sections of the wings of a flying wing aircraft, we used the constructal law and the concept of the flow of stresses in this paper. The results indicate that the aeroelastic stability of a flying wing aircraft is substantially influenced by the configuration of the wing's cross-section. This paper presents how the flow of stresses in the stress-carrying pathways in the lead-lag direction ($\mathbf{b}_2$) and the stress-carrying pathways in the plunge direction ($\mathbf{b}_3$) affect the stability of a flying wing aircraft. While the total cross-sectional mass remains constant, we reduce mass from the strip in the $\mathbf{b}_2$ direction and add them into branches in the $\mathbf{b}_3$ direction. We designed cases V and VI by inspiring from brirds' wing by focusing in the $\mathbf{b}_3$ direction.

According to the findings, σ_{11} and Von Mises stresses are essential for the prediction of aircraft aeroelastic instabilities. Stresses flow mainly in the plunge direction ($\mathbf{b}_3$) throughout the cross-section of the wing, which is the principal stress-carrying pathway and plays a significant role in the flow of stresses affecting the aeroelastic stability of the flying wing aircraft. The cases with higher flutter speed are associated with cross-sectional patterns that have the smoothest distribution of stresses in the pathways orientated in the plunge direction of the airfoil. It is demonstrated that sharp-edged shapes cause stress concentrates in the wing cross-section and reduce flutter speed. On the other hand, the curved edges improve the flutter speed and make the flow of stresses smoother.

VI. Acknowledgments

The U.S. National Science Foundation (NSF) supports Professor Mardanpour's research.

References

[1] Mardanpour, P., Izadpanahi, E., Rastkar, S., Lorente, S., and Bejan, A., "Constructal Design of Aircraft: Flow of Stresses and Aeroelastic Stability," *AIAA Journal*, 2018, pp. 1–13.

[2] Bejan, A., and Lorente, S., "Constructal law of design and evolution: Physics, biology, technology, and society," *Journal of Applied Physics*, Vol. 113, No. 15, 2013, pp. –. doi:10.1063/1.4798429.

[3] Bejan, A., "Constructal-theory network of conducting paths for cooling a heat generating volume," *International Journal of Heat and Mass Transfer*, Vol. 40, No. 4, 1997, pp. 799–816.

[4] Bejan, A., "Shape and Structure, from Engineering to Nature, Cambridge University Press, Cambridge, UK, 2000," ????

[5] Bejan, A., and Lorente, S., "Design with constructal theory," 2008.

[6] Bejan, A., Gunes, U., and Sahin, B., "The evolution of air and maritime transport," *Applied Physics Reviews*, Vol. 6, No. 2, 2019, p. 021319.

[7] Bejan, A., Charles, J., and Lorente, S., "The evolution of airplanes," *Journal of Applied Physics*, Vol. 116, No. 4, 2014, p. 044901.

[8] Bejan, A., Gunes, U., Charles, J., and Sahin, B., "The fastest animals and vehicles are neither the biggest nor the fastest over lifetime," *Scientific reports*, Vol. 8, No. 1, 2018, pp. 1–11.

[9] Chen, R., Wen, C., Lorente, S., and Bejan, A., "The evolution of helicopters," *Journal of Applied Physics*, Vol. 120, No. 1, 2016, p. 014901.

[10] Bejan, A., Charles, J. D., and Lorente, S., "The evolution of airplanes," *Journal of Applied Physics*, Vol. 116, No. 4, 2014, pp. –. doi:10.1063/1.4886855.

[11] Bejan, A., Charles, J., Lorente, S., and Dowell, E., "Evolution of airplanes, and What price speed?" *AIAA Journal*, Vol. 54, No. 3, 2016, pp. 1120–1123. doi:10.2514/1.J054481.

[12] Chen, R., Wen, C. Y., Lorente, S., and Bejan, A., "The evolution of helicopters," *Journal of Applied Physics*, Vol. 120, No. 1, 2016. doi:10.1063/1.4954976.

[13] Imumbhon, J. O., Alam, M. D., and Cao, Y., "Design and structural analyses of a reciprocating S1223 high-lift wing for an RA-driven VTOL UAV," *Aerospace*, Vol. 8, No. 8, 2021, p. 214.

[14] Alam, M. D., and Cao, Y., "Static and modal analysis of a crankshaft reciprocating driver for reciprocating-airfoil (RA) driven VTOL aircraft," *Mechanics Based Design of Structures and Machines*, 2021, pp. 1–16.

[15] Schuhmacher, G., Murra, I., Wang, L., Laxander, A., O'Leary, O., and Herold, M., "Multidisciplinary design optimization of a regional aircraft wing box," *9th AIAA/ISSMO Symposium on Multidisciplinary Analysis and Optimization*, 2002, p. 5406.

[16] Rao, J., Kiran, S., Kamesh, J., Padmanabhan, M. A., and Chandra, S., "Topology optimization of aircraft wing," *Journal of Aerospace Science and Technologies*, Vol. 61, No. 3, 2009, p. 402.

[17] Zhu, J.-H., Zhang, W.-H., and Xia, L., "Topology optimization in aircraft and aerospace structures design," *Archives of Computational Methods in Engineering*, Vol. 23, No. 4, 2016, pp. 595–622.

[18] Moshtaghzadeh, M., Izadpanahi, E., Bejan, A., and Mardanpour, P., "Evolutionary Aeroelastic Design of Flying-Wing Cross Section," *AIAA Journal*, 2021, pp. 1–12.

[19] Lorente, S., Lee, J., and Bejan, A., "The "flow of stresses" concept: The analogy between mechanical strength and heat convection," *International Journal of Heat and Mass Transfer*, Vol. 53, No. 15-16, 2010, pp. 2963–2968. doi: 10.1016/j.ijheatmasstransfer.2010.03.038.

[20] Lorente, S., Lee, J., and Bejan, A., "The "flow of stresses" concept: the analogy between mechanical strength and heat convection," *International Journal of Heat and Mass Transfer*, Vol. 53, No. 15-16, 2010, pp. 2963–2968.

[21] Izadpanahi, E., Rastkar, S., and Mardanpour, P., "Constructal Design of Flying Wing Aircraft: Curved and Swept Configurations," *AIAA Journal*, 2019, pp. 1–16.

[22] Izadpanahi, E., Moshtaghzadeh, M., Radnezhad, H. R., and Mardanpour, P., "Constructal approach to design of wing cross-section for better flow of stresses," *AIAA Scitech 2020 Forum*, 2020, p. 0275.

[23] Patil, M. J., and Hodges, D. H., "Flight dynamics of highly flexible flying wings," *Journal of Aircraft*, Vol. 43, No. 6, 2006, pp. 1790–1799. doi:10.2514/1.17640.

[24] Chang, C.-S., Hodges, D. H., and Patil, M. J., "Flight dynamics of highly flexible aircraft," *Journal of Aircraft*, Vol. 45, No. 2, 2008, pp. 538–545. doi:10.2514/1.30890.

[25] Hodges, D. H., "Geometrically exact, intrinsic theory for dynamics of curved and twisted anisotropic beams," *AIAA journal*, Vol. 41, No. 6, 2003, pp. 1131–1137. doi:10.2514/2.2054.

[26] Peters, D. A., Karunamoorthy, S., and Cao, W.-M., "Finite state induced flow models. I-Two-dimensional thin airfoil," *Journal of Aircraft*, Vol. 32, No. 2, 1995, pp. 313–322. doi:10.2514/3.46718.

[27] Sotoudeh, Z., Hodges, D. H., and Chang, C.-S., "Validation studies for aeroelastic trim and stability of highly flexible aircraft," *Journal of Aircraft*, Vol. 47, No. 4, 2010, pp. 1240–1247. doi:10.2514/1.46974.

[28] Timoshenko, S. P., and Gere, J. M., "Theory of elastic stability second edition," *McCraw-Hill Book Company: New York*, 1961.

[29] Simitses, G. J., and Hodges, D. H., *Fundamentals of structural stability*, Butterworth-Heinemann, 2006.

[30] Goland, M., and Luke, Y., "The flutter of a uniform wing with tip weights," *Journal of Applied Mechanics*, Vol. 15, No. 1, 1948, pp. 13–20.

[31] Dowell, E., Traybar, J., and Hodges, D. H., "An experimental-theoretical correlation study of non-linear bending and torsion deformations of a cantilever beam," *Journal of Sound and Vibration*, Vol. 50, No. 4, 1977, pp. 533–544. doi: 10.1016/0022-460X(77)90501-6.

[32] Bauchau, O. A., and Kang, N., "A multibody formulation for helicopter structural dynamic analysis," *Journal of the American Helicopter Society*, Vol. 38, No. 2, 1993, pp. 3–14. doi:10.4050/JAHS.38.3.

[33] Bauchau, O. A., "Computational schemes for flexible, nonlinear multi-body systems," *Multibody System Dynamics*, Vol. 2, No. 2, 1998, pp. 169–225. doi:10.1023/A:100971081.

[34] Saberi, H., Khoshlahjeh, M., Ormiston, R., and Rutkowski, M., "RCAS overview and application to advanced rotorcraft problems," *4th Decennial Specialists' Conference on Aeromechanics*, 2004.

[35] Mardanpour, P., Hodges, D. H., Neuhart, R., and Graybeal, N., "Engine placement effect on nonlinear trim and stability of flying wing aircraft," *Journal of Aircraft*, Vol. 50, No. 6, 2013, pp. 1716–1725. doi:10.2514/1.C031955.

[36] Hodges, D. H., "Nonlinear composite beam theory," *Progress in astronautics and aeronautics*, Vol. 213, 2006, p. 304.

[37] Yu, W., Volovoi, V. V., Hodges, D. H., and Hong, X., "Validation of the variational asymptotic beam sectional analysis," *AIAA journal*, Vol. 40, No. 10, 2002, pp. 2105–2112.

[38] Yu, W., Hodges, D. H., and Ho, J. C., "Variational asymptotic beam sectional analysis–an updated version," *International Journal of Engineering Science*, Vol. 59, 2012, pp. 40–64.

[39] Yu, W., and Hodges, D. H., "Generalized Timoshenko theory of the variational asymptotic beam sectional analysis," *Journal of the American Helicopter Society*, Vol. 50, No. 1, 2005, pp. 46–55.

[40] Geuzaine, C., and Remacle, J.-F., "Gmsh: A 3-D finite element mesh generator with built-in pre-and post-processing facilities," *International journal for numerical methods in engineering*, Vol. 79, No. 11, 2009, pp. 1309–1331.

[41] Müller, W., and Patone, G., "Air transmissivity of feathers," *The Journal of experimental biology*, Vol. 201, No. 18, 1998, pp. 2591–2599.

[42] Mardanpour, P., Izadpanahi, E., Rastkar, S., Lorente, S., and Bejan, A., "Constructal Design of Aircraft: Flow of Stresses and Aeroelastic Stability," *AIAA Journal*, Vol. 57, No. 10, 2019, pp. 4393–4405.

[43] Izadpanahi, E., Rastkar, S., and Mardanpour, P., "Constructal Design of Flying Wing Aircraft: Curved and Swept Configurations," *AIAA Journal*, Vol. 57, No. 12, 2019, pp. 5527–5542.

[44] Mardanpour, P., Izadpanahi, E., Powell, S., Rastkar, S., and Bejan, A., "Inflected wings in flight: Uniform flow of stresses makes strong and light wings for stable flight," *Journal of Theoretical Biology*, Vol. 508, 2021, p. 110452.